Pramāṇa – J. Phys., Vol. 29, No. 2, August 1987, pp. 167–182. © Printed in India.

Holographic grating based Ebert spectrograph

N C DAS and M V R K MURTY*

Spectroscopy Division, Bhabha Atomic Research Centre, Bombay 400 085, India
*Physics Department, Alabama Agricultural and Mechanical University, Alabama 35762, USA

MS received 23 February 1987; revised 21 May 1987

Abstract. In this paper we discuss the aberration properties and design procedure of in-plane Ebert spectrograph using conventional as well as holographic diffraction gratings. In both cases the gratings are situated at the well-known $\sqrt{3}$-position so that the spectrum can be recorded on a flat surface. It has been found that the holographic grating system has better resolution than the conventional grating system. The design parameters of a medium sized holographic grating spectrograph in which a concave spherical mirror is mounted in the off-axis configuration have been specified. The performance of the spectrograph has been evaluated by plotting spot diagram.

Keywords. Ebert spectrograph; holographic grating; aberration; interference fringes.

PACS Nos 7·65; 42·40; 42·80

1. Introduction

Recently we have reported the aberration properties and design method of flat field spectrograph (Das and Murty 1986) using a convex holographic diffraction grating and a concave mirror. In this paper we discuss the aberration properties and design principles of an Ebert type flat field spectrograph, which uses a plane holographic diffraction grating as the dispersing element. Ebert system (Ebert 1889) was first revived by Fastie (1952, 1953) whose basic geometry is illustrated in figure 1. This is basically an in-plane system in which the source point S_1 and the image point S_2 are located at the two ends of a plane grating G equidistant from the axis.

The extensive research work on the imaging properties of Ebert system has been reviewed by Welford (1965). The aberration properties of Ebert system may be summarized as follows.

The system suffers from spherical aberration, coma and astigmatism (Rosendahl 1962). Only the zero-order image is free from coma because of perfect symmetry. Coma, however, increases for spectral images which are focused on both sides of the zero order image. Both spherical aberration and coma can be eliminated by using large f-number (Murty 1974) system. By introducing asphericity (Murty 1962) on the concave mirror and the plane grating it is possible to design a small f-number instrument which is completely free from coma and spherical aberration at least for one wavelength.

In the case of scanning type instrument the effect of astigmatism can be eliminated by using curved slits (Kudo 1960, 1965; Megill and Droppleman 1962) at the source and the image points. Both coma and astigmatism can, however, be eliminated by using a

concentric system (Horwitz 1974) using additional plane mirrors as folding elements.

The spectrum can be recorded on a flat surface when the plane grating is located at the $\sqrt{3}$-position (Khrshnanovskii 1960; Sassa 1961; Mielenz 1964) for which the distance between the plane grating and the centre of curvature of the concave mirror is $R/\sqrt{3}$, where R is the radius of the concave mirror.

The present system with a plane holographic grating and a moderate sized concave mirror in the off-axis configuration uses the in-plane geometry and will record a long range of spectral images on a standard photographic plate. Because of the method of construction for the holographic grating, at least one of the spectral images will be completely free from aberration.

2. Construction of the holographic grating

In order to discuss the construction principle of the holographic grating let us refer figure 1. Two coherent sources are located at the two points S_1 and S_2 which are equidistant from the axis AA' and lie on the focal plane of the concave spherical mirror M. Light diverging from the two coherent sources are collimated by the concave mirror and produce interference fringes on the glass plate G which is coated with photo-resistant and is kept at the $\sqrt{3}$-position (Khrshnanovskii 1960; Sassa 1961; Mielenz 1964) of the system. After exposure and development, the glass plate is coated with a reflecting material so that it behaves as a plane reflection grating when illuminated by a polychromatic beam of light. The grooves formed on the plane grating will slightly deviate from straight lines since the two interfering wavefronts are not exactly plane due to the inherent aberrations of the spherical mirror having finite aperture and off-axis illumination. Since the grooves will not be exactly straight the grating spacing throughout the area of the holographic grating will not be uniform.

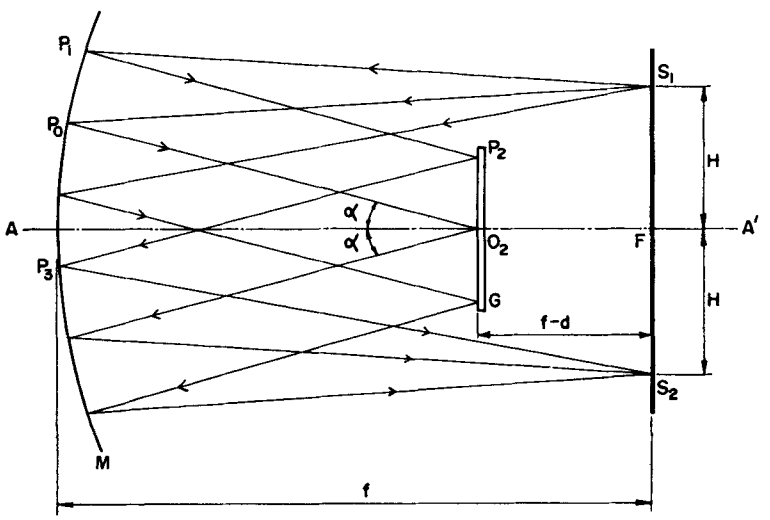

Figure 1. In-plane Ebert system consisting of concave mirror M and the plane grating G.

For recording the spectrum the plane holographic grating is mounted at its original recording position G and illuminated by a polychromatic beam of light diverging from one of the source points S_1 and collimated by the concave mirror M_1. Then from the holographic principle an aberration-free image of the constructing wavelength λ_0 will be formed at S_1 while the zero-order image will be formed at S_2. Images corresponding to other wavelengths will be focused on either side of S_1 and S_2 and they suffer from various types of aberrations.

3. Imaging principle of the holographic grating spectrograph

The principle of image formation by the spectrograph using concave mirror and plane holographic diffraction grating is illustrated in figure 2 where S_1 and S_2 represent the illuminating source and the zero order image respectively. The positive and the negative order spectral images for any wavelength λ will be focused at S' and S'_- respectively. Since the grating is located at the $\sqrt{3}$-position the spectrum will be formed on a flat surface which is perpendicular to the axis as well as the plane of the paper and passes through the focal point F of the concave mirror. Expression for the spectral image distance from the axis may be derived as follows.

Let us consider the central incident rays S_1P_0 and P_0O_2, which are also the directions of the diffracted rays for the constructing wavelength λ_0. The central diffracted rays for any other wavelength λ are denoted by $O_2P'_0$ and P'_0S'. Then the equation of diffraction for the constructing wavelength λ_0 is given by

$$2\sin\alpha = \lambda_0/\sigma_0, \tag{1}$$

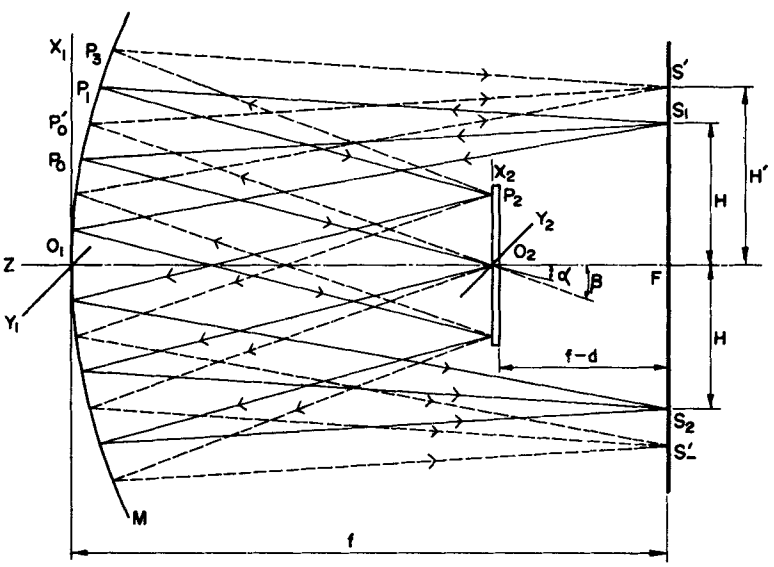

Figure 2. Diagram showing the imaging principle and co-ordinate systems of in-plane Ebert spectrograph in which S_1 and S_2 are the source and the zero order image respectively. S' and S'_- are the positive and the negative order spectral images respectively for any wavelength λ.

where α is the incident as well as the diffraction angle for the constructing wavelength λ_0 and σ_0 is the grating spacing at the central point O_2 of the holographic grating. Similarly the equation of diffraction for any other wavelength λ is given by

$$\sin\alpha+\sin\beta=\lambda/\sigma_0, \tag{2}$$

where β is the angle of diffraction for the wavelength λ. Eliminating σ_0 from (1) and (2), the diffraction equation for the wavelength λ may be written as

$$\sin\beta=[2(\lambda/\lambda_0)-1]\sin\alpha. \tag{3}$$

From simple geometrical considerations from figures 1 and 2 one may show that

$$\sin\alpha=H/(H^2+f^2)^{1/2}, \tag{4}$$

$$\sin\beta=H'/(H'^2+f^2)^{1/2}, \tag{5}$$

where f is the focal length of the concave mirror, H is the source distance from the axis and H' is the image distance for any wavelength λ from the axis. Taking the paraxial approximations of (4) and (5) and using (1) and (3) one can show that

$$1/\sigma_0=2(H/f)/\lambda_0, \tag{6}$$

$$H'=[2(\lambda/\lambda_0)-1]H. \tag{7}$$

Equations (6) and (7) give the nominal grating frequency and the spectral image distance in terms of the construction parameters of the holographic grating. Differentiating (7) with respect to λ the reciprocal linear dispersion of the system is given by

$$\mathrm{d}\lambda/\mathrm{d}H'=\lambda_0/2H. \tag{8}$$

It is to be noted that (1) gives the exact grating spacing σ_0 at the central point O_2 of the holographic grating. Grating spacing at some other point P_2 of the holographic grating will be slightly different from σ_0 since the grooves formed on the holographic grating will be slightly curved. Grooves formed on the holographic grating will be equispaced and straight only when the recording sources are very close to the axis and the light beams originating from the recording sources have small divergence angle so that the two interfering wavefronts reflected by the concave mirror are perfectly plane. Under this condition the holographic grating will be equivalent to a conventional plane grating having equispaced and straight rulings whose ruling spacing is given by (6). The expression for the exact grating spacing at any point P_2 of the holographic grating, when the recording wavefronts are not exactly plane due to finite aperture and source distance of the practical system, has been derived in the ray tracing scheme and it is given by (16) of Appendix 1.

4. Aberration properties

The aberration properties of the spectrograph have been studied by actual ray tracing. Referring to figures 1 and 2, the focal length of the concave mirror is assumed to be

unity and the grating is assumed to be located at the $\sqrt{3}$-position, so that the distance between the concave mirror and the grating is equal to 0·84. The source distance H from the axis has been decided on the basis of the desired value for the nominal grating frequency as specified by (6) and the available laser wavelengths for the constructing wavelength λ_0. A reasonable value of H suitable for constructing gratings with medium frequencies using existing laser wavelengths and their second harmonics is assumed to be 0·1, so that the field angle α is not very large.

Since the spectrum will be formed on a flat surface because of the particular choice of the grating position, we have evaluated only the broadening of the spectral images due to spherical aberration and coma. For this purpose, several tangential rays lying in the plane of dispersion and originating from the source point S_1, have been traced so that the full width of the grating is covered. Ray aberrations for various spectral images have been evaluated by simply computing the deviation of the ray intersection points on the focal plane from the ideal image point S' whose distance from the axis is represented by the paraxial equation (7). While computing the ray aberrations we have considered both the conventional plane grating having uniform grating spacing described by (6) and the plane holographic grating whose grating spacing varies throughout the entire area in accordance with (16) of Appendix 1.

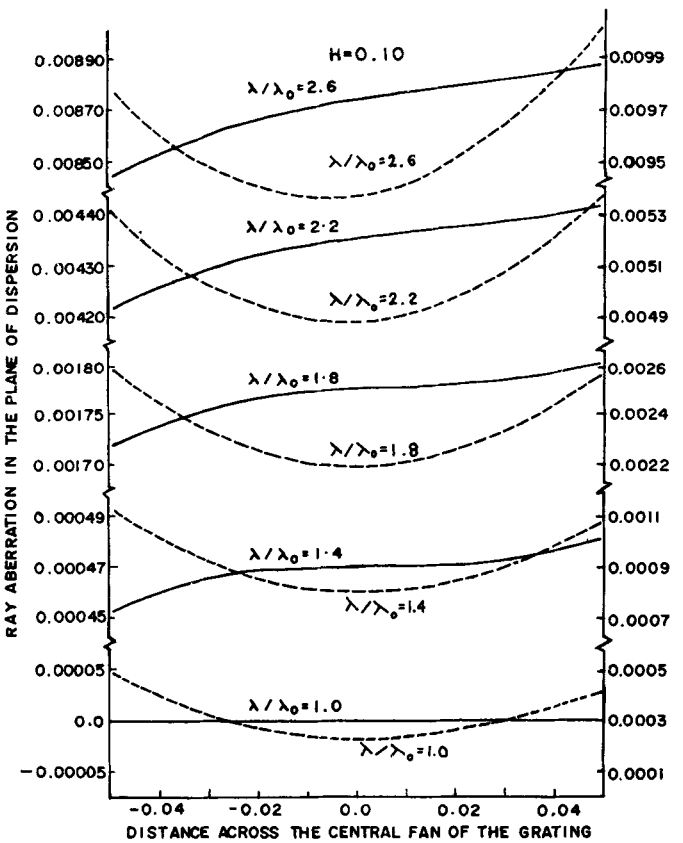

Figure 3. Typical ray aberration curves for positive order spectral images. The solid and the broken curves are drawn considering the holographic grating and the conventional grating respectively as the dispersing element.

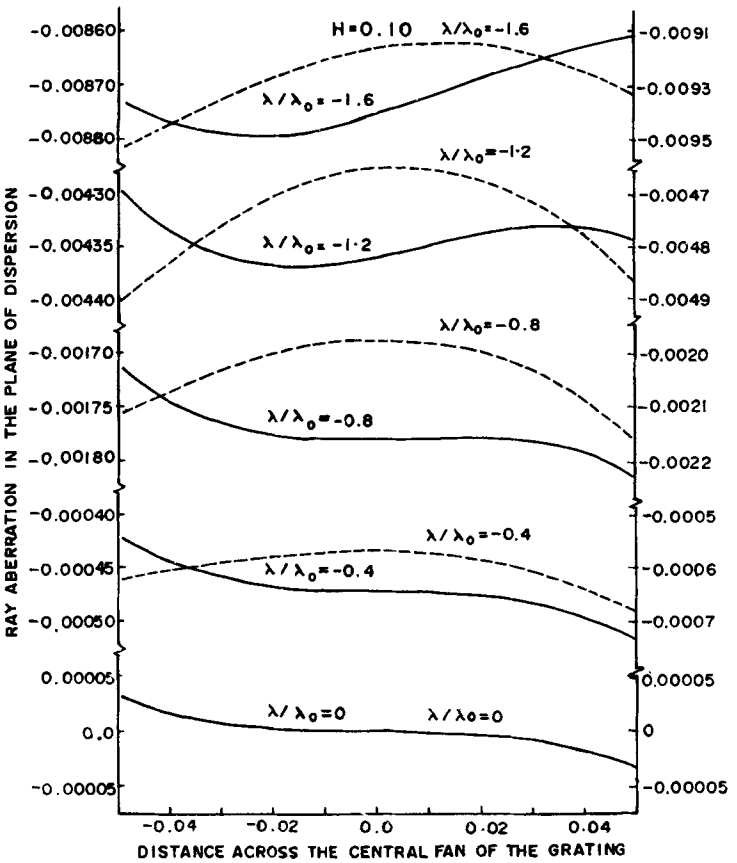

Figure 4. Typical ray aberration curves for negative order spectral images. The solid and the broken curves are drawn considering the holographic grating and the conventional grating respectively as the dispersing element.

Typical ray aberration curves for the positive and the negative order spectral images are shown in figures 3 and 4 respectively. In each figure the solid curves with ordinate scale in the left hand side describe the aberration of the holographic grating system and the broken curves with ordinate scale in the right hand side describe the aberration of the conventional grating system. It may be seen from figure 4 that the aberration curve for the zero order image is same for both the cases. Also, the zero order image suffers from spherical aberration only. For other wavelengths the holographic grating system suffers from less amount of aberration than the conventional grating system. Also, the holographic grating system forms an aberration-free image of the constructing wavelength λ_0 at the original source position whereas in the case of conventional grating system the littrow wavelength λ_0 which is also focused at the original source position suffers from finite amount of aberration. In the conventional grating system the littrow wavelength λ_0 suffers from more amount of aberration than the zero order image, since coma is additive in the case of the littrow wavelength λ_0, whereas it is completely absent in the zero order image due to perfect symmetry. Finally, in both the cases ray aberration increases when the wavelength shifts from the original source position as well as the zero order position.

In order to study the resolution properties of the spectral images, image blur

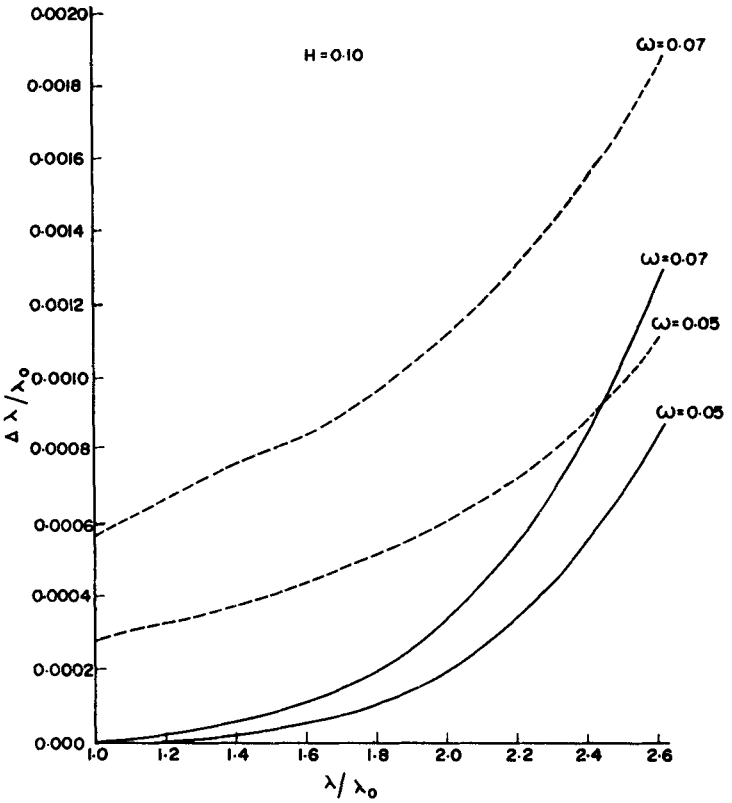

Figure 5. Resolution curves of positive order spectral images formed by the holographic grating and the conventional grating spectrograph for two different values of the grating width ω. Solid curves are for the holographic grating system and broken curves are for the conventional grating system.

corresponding to various wavelengths has been estimated from the ray aberration curves. Let us suppose that $\Delta H'$ is the image blur and $\Delta\lambda$ is the corresponding wavelength spread for any spectral image. Then from (8), the resolution of the spectrograph at any wavelength λ is given by

$$\Delta\lambda/\lambda_0 = \Delta H'/2H. \tag{9}$$

Using (9), the resolution of the spectral images has been computed and plotted against wavelength. Figures 5 and 6 show the resolution curves for the positive and the negative order spectral images respectively. The solid curves represent the resolution of the holographic grating system whereas the broken curves show the resolution of the conventional grating system. In each figure two curves have been plotted for two different values of the grating width ω. It may be seen that for the same grating width the holographic system shows better resolution properties than the conventional grating system. Further it may be seen that in the case of holographic grating system, the resolution of all wavelengths in the neighbourhood of the constructing wavelength λ_0 and the zero order image is relatively high compared to the conventional grating system, which shows poor resolution at the littrow wavelength λ_0 as well as its neighbouring wavelengths because of relatively large amount of aberration.

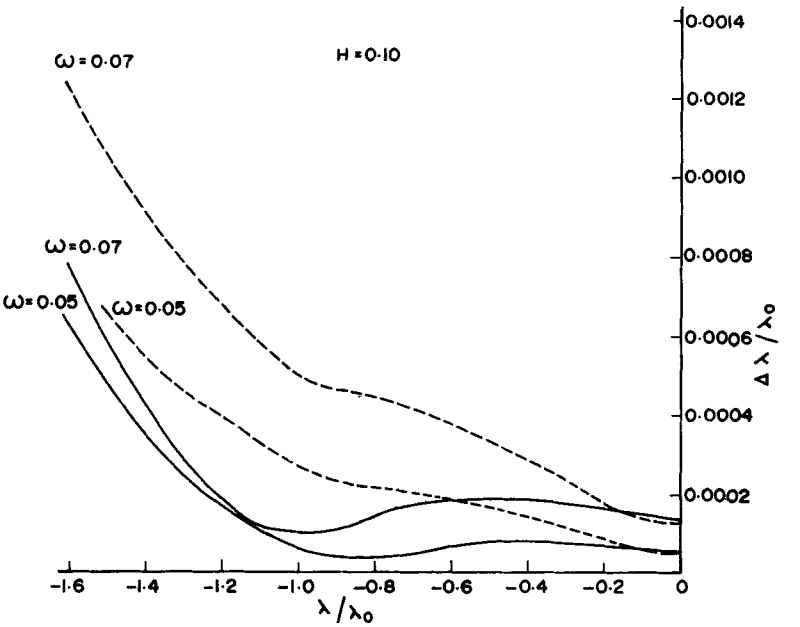

Figure 6. Resolution curves of negative order spectral images formed by the holographic grating and the conventional grating spectrograph for two different values of the grating width ω. Solid curves are for the holographic grating system and the broken curves are for the conventional grating system.

5. Practical spectrograph

A quantitative study of the aberration properties and the resolution of the spectrograph discussed above in case of two different grating widths is based on the assumption that (a) the focal length of the concave mirror is unity; (b) the distance between the concave mirror and the grating is 0·84; (c) the source distance from the axis is 0·1. All these parameters are to be scaled up by the focal length of the practical system. Out of the two values for the grating width, we shall consider the smallest value of 0·05 since the resolution of the spectrograph is comparatively high for this particular value of the grating width as shown by the curves drawn in figures 5 and 6.

Based on the above consideration, we have specified the following parameters for a medium sized spectrograph:

Focal length of the concave mirror	: 1000 mm
Grating distance from the concave mirror	: 840 mm
Source distance from the axis	: 100 mm
Grating size	: 50 × 50 mm
Speed of the spectrograph	: $f/14{\cdot}1$

The construction wavelength λ_0 for the holographic grating has been considered to be 3638 Å of argon ion laser or its second harmonic 1819 Å. Using (6) and (8) nominal grating frequency of the holographic grating and reciprocal linear dispersion of the instrument are obtained as follows:

Grating A:

Construction wavelength	: 3638 Å
Nominal grating frequency	: 550 lines/mm
Reciprocal linear dispersion	: 18·2 Å/mm

Grating B:

Construction wavelength	: 1819 Å
Nominal grating frequency	: 1100 lines/mm
Reciprocal linear dispersion	: 9·1 Å/mm

In order to specify the diameter of the concave mirror required for constructing the holographic grating, let us refer figure 1. It may be seen that the incident height of the central ray S_1P_0 on the mirror surface is given by

$$X_0 = d\tan\alpha. \tag{10}$$

Then for constructing a grating having diagonal length D, the required diameter of the concave mirror is given by

$$D_m = 2X_0 + D. \tag{11}$$

Using the paraxial approximations of (4) and (10), equation (11) may be written as

$$D_m = 2d(H/f) + D. \tag{12}$$

Since all the parameters of (12) have already been specified for a practical system, we may further specify

Diameter of the concave mirror for constructing the grating: 240 mm

Table 1. Resolution of the practical spectrograph at various wavelengths using low frequency holographic or conventional grating having construction or littrow wavelength λ_0 equal to 3638 Å.

λ_0 (Å)	λ (Å)	$(\Delta\lambda)_H$ (Å)	$(\Delta\lambda)_C$ (Å)	$(\Delta\lambda)_0$ (Å)
3638	4000	0·02	1·14	0·15
	5000	0·07	1·36	0·18
	6000	0·25	1·64	0·22
	7000	0·58	2·05	0·25
	8000	1·24	2·64	0·29
	−1000	0·27	0·41	0·04
	−2000	0·26	0·64	0·07
	−3000	0·13	0·77	0·11
	−4000	0·40	1·18	0·15

$(\Delta\lambda)_H$, $(\Delta\lambda)_C$ and $(\Delta\lambda)_0$ denote the resolution of the holographic grating system, the conventional grating system and the aberration free system respectively. Negative wavelengths indicate that the spectral images are formed in the negative order.

Table 2. Resolution of the practical spectrograph at various wavelengths using high frequency holographic or conventional grating having construction or littrow wavelength λ_0 equal to 1819 Å. The rest is same as in table 1.

λ_0 (Å)	λ (Å)	$(\Delta\lambda)_H$ (Å)	$(\Delta\lambda)_C$ (Å)	$(\Delta\lambda)_0$ (Å)
1819	2000	0·01	0·57	0·04
	2500	0·04	0·68	0·05
	3000	0·13	0·82	0·06
	3500	0·29	1·02	0·06
	4000	0·62	1·32	0·07
	−1000	0·13	0·32	0·02
	−1500	0·06	0·39	0·03
	−2000	0·20	0·59	0·04

Tables 1 and 2 show the actual resolution of the spectrograph using holographic gratings *A* and *B* and two conventional gratings whose constant ruling frequencies are equal to the nominal frequencies of the gratings *A* and *B*. In both the tables $(\Delta\lambda)_H$ and $(\Delta\lambda)_C$ denote the aberration limited resolution of the spectrograph using the holographic grating and the conventional grating respectively and $(\Delta\lambda)_0$ indicates diffraction limited resolution of an ideal system. The actual values of the wavelength and the resolution have been obtained by scaling up the wavelength ratio λ/λ_0 and the resolution $\Delta\lambda/\lambda_0$ plotted in figures 5 and 6, by the construction or the littrow wavelength λ_0. For this purpose we have considered the resolution curve corresponding to the normalized grating width of 0·05 only which is equivalent to 50 mm grating width for the practical spectrograph. It is evident from tables 1 and 2 that for almost all wavelengths the resolution of the holographic grating spectrograph is very close to the resolution of the diffraction limited system, unlike the resolution of the conventional grating spectrograph.

It is evident that if one wishes to record both positive and negative order spectral images using a single concave mirror as the collimating and the focusing element, a large diameter for the concave mirror will be required since we have considered the in-plane geometry of the spectrograph. So the most practical proposition is to record the positive order spectrum only and to use gratings *A* and *B* in succession to record the visible and the UV wavelengths respectively. For this purpose the concave mirror should be mounted in the off-axis configuration as shown in figure 7. Although, the system is basically a littrow arrangement, the aberrations of the spectral images will be less due to the use of holographic grating as confirmed by our computational results. Referring to figure 7, the incident height of the central ray S_1P_0 on the mirror surface has already been specified by (10) and that of the central diffracted ray $O_2P'_0$ is given by

$$X'_0 = d\tan\beta. \tag{13}$$

using (7) and the paraxial approximations of (4) and (5), we have from (10) and (13)

$$X'_0 - X_0 = 2d(H/f)(\lambda/\lambda_0 - 1). \tag{14}$$

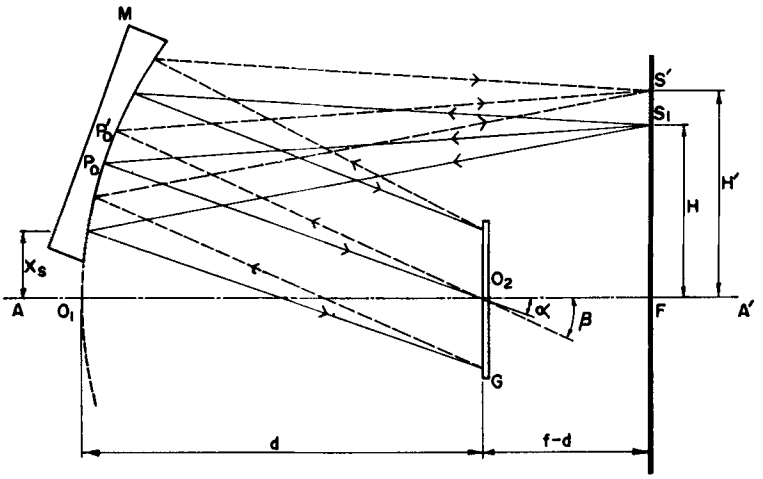

Figure 7. Schematic diagram of the practical spectrograph using the off-axis concave mirror M and the holographic grating G.

Thus the mirror diameter required to focus the wavelength range of λ_0 to λ using a grating of diagonal length D is given by

$$D_m = X'_0 - X_0 + D. \tag{15}$$

Referring to figure 7, the off-axis shift and off-axis angle θ (not shown in figure) are given by

$$X_S = X_0 - D/2, \tag{16}$$

$$\tan\theta = (X_S + D_m/2)/d. \tag{17}$$

using (14) to (17) we may specify the following parameters for the concave mirror M to be used in the holographic grating spectrograph as per geometry of figure 7.

Mirror diameter for recording	
Visible or UV region of the spectrum	: 270 mm
Off-axis shift of the mirror	: 50 mm
Off-axis angle of the mirror	: 11·8°.

It is to be noted that the mirror diameter required to construct the grating and that required to record the spectrum are slightly different. Instead of using two different mirrors, a single mirror having diameter of 250 mm will be quite adequate for both the purpose.

The practical spectrograph whose basic geometry has been shown in figure 7 and whose geometrical parameters have already been specified, has been evaluated by plotting the spot diagram. For this purpose a large number of rays originating from the source point S_1 and covering the full aperture of the grating have been traced and the co-ordinates of the ray interesection points on the focal plane have been found out. Figures 8 and 9 show the spot sizes at various wavelengths when the spectrograph uses the low frequency holographic grating A having nominal grating frequency of

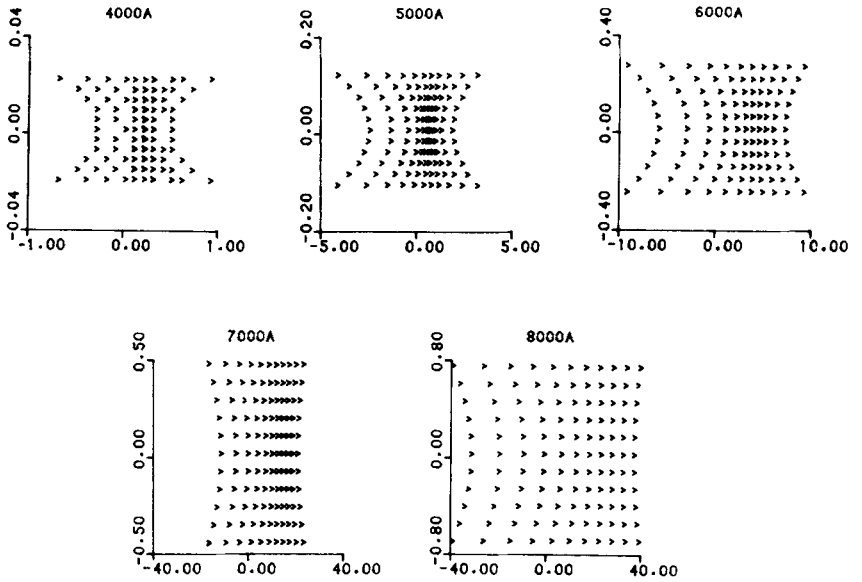

Figure 8. Spot diagram of the holographic grating spectrograph at various wavelengths using point source. Horizontal axis represents spectral image blur in micrometer and the vertical axis represents the length of the spectral image in mm.

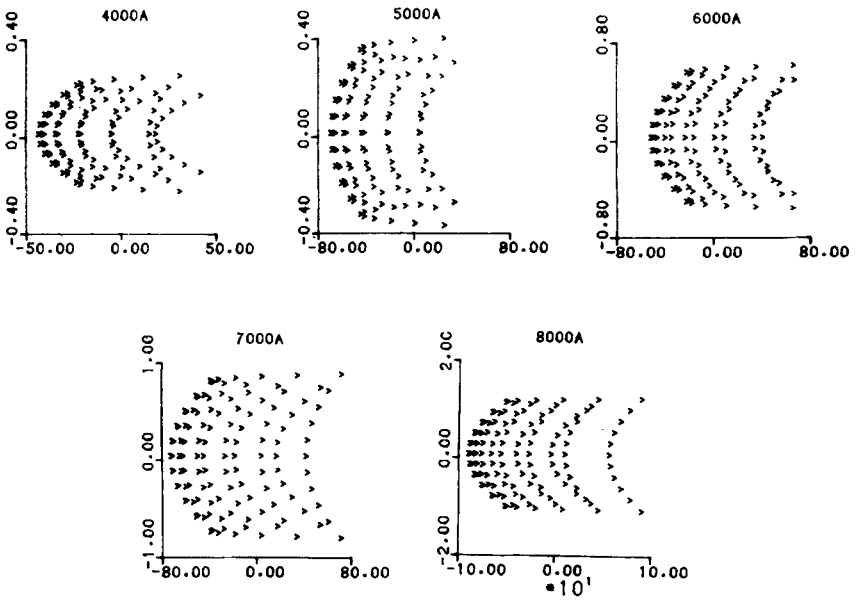

Figure 9. Spot diagram of the conventional grating spectrograph at various wavelengths using point source. Horizontal axis represents spectral image blur in micrometer and the vertical axis represents the length of the spectral image in mm.

550 lines/mm and a conventional grating with the same frequency respectively. The horizontal axis of the spot diagram represents the broadening of the spectral image in micrometer whereas the vertical axis shows the lengthening of the spectral image in mm. While using the high frequency grating *B*, the spot diagram will remain unchanged

in both cases except that the wavelength specified on the top of each diagram should be halved. It may be seen from the spot diagram that both lengthening and broadening of the spectral images formed by the holographic grating spectrograph will be much less as compared to the conventional grating spectrograph.

Finally we may conclude that a medium sized spectrograph having flat field, moderate dispersion and resolution properties throughout the UV-visible region of the spectrum may be constructed following the geometry of in-plane Ebert system and using a plane holographic diffraction grating whose construction parameters have already been discussed.

Acknowledgements

The authors thank Dr S L N G Krishnamachari for his interest in this work and Mr R D'Souza for technical help.

Appendix 1: Ray tracing scheme of the spectrograph

Figure 2 shows the ray paths and the co-ordinate systems for the ray incident points on the concave mirror M and the plane holographic grating G. Let us suppose that R is the radius of the concave mirror and d is the axial distance between the concave mirror and the holographic grating. A typical ray S_1P_1 originating from the source point S_1 is incident on the concave mirror at the point P_1 and gets reflected in the direction of P_1P_2. Since the construction geometry of the holographic grating shown in figure 1 perfectly matches the reconstruction geometry represented by figure 2, the diffracted ray for the constructing wavelength λ_0 will retrace the original incident path P_2P_1 and P_1S_1 to meet the original source point S_1. For any other wavelength λ, the diffracted ray will follow the path P_2P_3 and P_2S' to meet the focal plane at the point S'. Following Spencer and Murty (1962) the direction cosines of the rays S_1P_1, P_1P_2, P_2P_3 and P_2S' and the co-ordinates of the ray incident points P_1, P_2 and P_3 are formulated based on the following scheme.

$(H,O,R/2)$—co-ordinates of the source point S_1 with respect to the origin at O_1 which is the pole of the concave mirror M_1.
(X_1,Y_1,Z_1)—co-ordinates of the point P_1 with respect to the origin at O_1.
(X_2,Y_2,Z_2)—co-ordinates of the point P_2 with respect to the origin at O_2 which is the central point of the plane grating.
(X_3,Y_3,Z_3)—co-ordinates of the point P_3 with respect to the origin at O_1.
(X',Y',Z')—co-ordinates of the image point S' with respect to the origin at O_1.

Based on the above scheme the following equations are obtained.
(i) Path length S_1P_1:

$$S_1P_1=[(X_1-H)^2+Y_1^2+(Z_1-R/2)^2]^{1/2};$$

$$Z_1=R-[R^2-(X_1^2+Y_1^2)]^{1/2}. \tag{A1}$$

(ii) Direction cosines of the ray S_1P_1:

$$k_1=(X_1-H)/S_1P_1;\quad l_1=Y_1/S_1P_1;\quad m_1=(Z_1-R/2)/S_1P_1. \tag{A2}$$

(iii) Direction cosines of the normal at P_1:

$$K_1=-X_1/R;\quad L_1=-Y_1/R;\quad M_1=1-Z_1/R. \tag{A3}$$

(iv) Direction cosines of the reflected ray P_1P_2:

$$k_2=k_1-2a_1K_1;\quad l_2=l_1-2a_1L_1;\quad m_2=m_1-2a_1M_1; \tag{A4}$$

$$a_1=(k_1K_1+l_1L_1+m_1M_1)/(K_1^2+L_1^2+M_1^2). \tag{A5}$$

(v) Path length P_1P_2:

$$D_2=(d-Z_1)/m_2. \tag{A6}$$

(vi) Co-ordinates of the P_2:

$$X_2=X_1+k_2D_2;\quad Y_2=Y_1+l_2D_2;\quad Z_2=Z_1+m_2D_2-d. \tag{A7}$$

(vii) Direction cosines of the normal at P_2:

$$K_2=0;\quad L_2=0;\quad M_2=1{\cdot}0. \tag{A8}$$

(viii) Direction cosines of the diffracted ray P_2P_3:

$$k_3=k_2-\Lambda u_2+\Gamma_f K_2;\quad l_3=l_2-\Lambda v_2+\Gamma_f L_2;$$

$$m_3=m_2-\Lambda w_2+\Gamma_f M_2. \tag{A9}$$

$$\Lambda=\lambda/\sigma, \tag{A10}$$

where σ is the local grating spacing at the point P_2. The significance of the groove parameters (u_2, v_2, w_2) and the multiplier Γ_f has been discussed by Spencer and Murty (1962). It has been shown that for any type of grating the groove parameters satisfy the following equations

$$K_2u_2+L_2v_2+M_2w_2=0. \tag{A11}$$

$$u_2^2+v_2^2+w_2^2=1{\cdot}0. \tag{A12}$$

(ix) Groove parameters and local grating spacing of the holographic grating:

In order to obtain the expression for the exact grating spacing at any point P_2 of the holographic grating let us apply the diffraction equations (9) to the incident ray P_1P_2 and the diffracted ray P_2P_1 for the constructing wavelength λ_0. Since the direction cosines of these two rays are equal in magnitude and opposite in sign we have from (9)

$$-k_2=k_2-\Lambda_0u_2+\Gamma_0K_2;\quad -l_2=l_2-\Lambda_0v_2+\Gamma_0L_2;$$

$$-m_2=m_2-\Lambda_0w_2+\Gamma_0M_2. \tag{A13}$$

$$\Lambda_0 = \lambda_0/\sigma, \tag{A14}$$

where Γ_0 is the value of the multiplier Γ_f when one considers the constructing wavelength λ_0. Using (11) to (14) one may obtain the following expressions for multiplier the Γ_0, the local grating spacing σ and the groove parameters (u_2, v_2, w_2) for the holographic grating as follows

$$\Gamma_0 = -2(k_2K_2 + l_2L_2 + m_2M_2)/(K_2^2 + L_2^2 + M_2^2). \tag{A15}$$

$$\Lambda_0 = [(2k_2 + \Gamma_0K_2)^2 + (2l_2 + \Gamma_0L_2)^2 + (2m_2 + \Gamma_0M_2)^2]^{1/2}. \tag{A16}$$

$$u_2 = (2k_2 + \Gamma_0K_2)/\Lambda_0; \quad v_2 = (2l_2 + \Gamma_0L_2)/\Lambda_0$$

$$w_2 = (2m_2 + \Gamma_0M_2)/\Lambda_0. \tag{A17}$$

(x) Groove parameters for the conventional gratings:

Following Spencer and Murty (1962) for conventional reflection grating having equispaced and straight rulings groove parameters are given by,

$$u_2 = -1/[1 + K_2^2/(L_2^2 + M_2^2)]^{1/2}; \quad v_2 = -K_2L_2u_2/(L_2^2 + M_2^2);$$

$$w_2 = -K_2M_2u_2/(L_2^2 + M_2^2). \tag{A18}$$

(xi) Multiplier Γ_f:

The multiplier Γ_f in (9) can be determined by the following iteration formula,

$$\Gamma_{n+1} = (\Gamma_n^2 - b')/2(\Gamma_n + a_2) \tag{A19}$$

where a_2 and b' are given by

$$a_2 = (k_2K_2 + l_2L_2 + m_2M_2)/(K_2^2 + L_2^2 + M_2^2). \tag{A20}$$

$$b' = [\Lambda^2 - 2\Lambda(k_2u_2 + l_2v_2 + m_2w_2)]/(K_2^2 + L_2^2 + M_2^2). \tag{A21}$$

In order to use the iteration equation (19), the first approximation of Γ_n may be assumed to be

$$\Gamma_1 = b'/2a_2 - 2a_2. \tag{A22}$$

(xii) Path length P_2P_3:

$$D_3 = -B + \sqrt{(B^2 - C)}. \tag{A23}$$

$$\mathrm{B} = k_3X_2 + l_3Y_2 + m_3(d - R). \tag{A24}$$

$$\mathrm{C} = X_2^2 + Y_2^2 + d(d - 2R). \tag{A25}$$

(xiii) Co-ordinates of the point P_3:

$$X_3 = X_2 + D_3k_3; \quad Y_3 = Y_2 + D_3l_3; \quad Z_3 = d + D_3m_3. \tag{A26}$$

(xiv) Direction cosines of the normal at the point P_3:

$$K_3 = -X_3/R; \quad L_3 = -Y_3/R; \quad M_3 = 1 - Z_3/R. \tag{A27}$$

(xv) Direction cosines of the reflected ray P_3S':

$$k'_3 = k_3 - 2a_3K_3; \quad l'_3 = l_3 - 2a_3L_3; \quad m'_3 = m_3 - 2a_3M_3. \tag{A28}$$

$$a_3 = (k_3K_3 + l_3L_3 + m_3M_3)/(K_3^2 + L_3^2 + M_3^2). \tag{A29}$$

(xvi) Path length P_3S':

$$D'_3 = (R - 2Z_3)/2m'_3. \tag{A30}$$

(xvii) Co-ordinates of the point S':

$$X' = X_3 + k'_3D'_3; \quad Y' = Y_3 + l'_3D'_3; \quad Z' = R/2. \tag{A31}$$

References

Das N C and Murty M V R K 1986 *Pramana–J. Phys.* **27** 171
Ebert H 1889 *Wied. Ann.* **38** 489
Fastie W G 1952 *J. Opt. Soc. Am.* **42** 641, 647
Fastie W G 1953 *J. Opt Soc. Am.* **43** 1174
Horwitz J W 1974 *Opt. Acta* **21** 169
Kudo K 1960 *Sci. Light (Tokyo)* **9** 1
Kudo K 1965 *J. Opt. Soc. Am.* **55** 150
Khrshnanovskii S A 1960 *Opt. Spectrosc.* **9** 207
Murty M V R K 1962 *J. Opt. Soc. Am.* **52** 515
Murty M V R K 1974 *Opt. Engg.* **13** 23
Megill L R and Droppleman L 1962 *J. Opt. Soc. Am.* **52** 258
Mielenz K D 1964 *J. Res. NBS (Engg. and Instrum.)* **C68** 205
Rosendahl G R 1962 *J. Opt. Soc. Am.* **52** 412
Sassa N 1961 *Sci. Light (Tokyo)* **10** 53
Spencer G H and Murty M V R K 1962 *J. Opt. Soc. Am.* **52** 672
Welford W T 1965 *Progress in Optics* (ed.) E Wolf (Amsterdam: North-Holland) Vol. IV p 241